Solar Phys (2007) 241: 145–169
DOI 10.1007/s11207-007-0258-y

Fine Structure of Solar Radio Bursts Observed at Decametric and Hectometric Waves

G.P. Chernov · M.L. Kaiser · J.-L. Bougeret · V.V. Fomichev · R.V. Gorgutsa

Received: 4 July 2006 / Accepted: 19 January 2007 /
Published online: 21 March 2007

Abstract The analysis of *WIND/WAVES* RAD2 spectra with fine structure in the form of different fibers in 14 events covering 1997 – 2005 is carried out. A splitting of broad bands of the interplanetary (IP) type II bursts into narrow band fibers of different duration is observed. The instantaneous-frequency bandwidth of fibers is stable: 200 – 300 kHz for slow-drifting fibers in type II bursts, and 700 – 1000 kHz for fast-drifting fibers in type II + IV (continuum). Intermediate drift bursts (IDB or fiber bursts) and zebra patterns with variable frequency drift of stripes, typical for the metric range, were not found. Comparison of spectra with the Solar and Heliospheric Observatory/Large Angle and Spectrometric Coronagraph (SOHO/LASCO C2) images shows a connection of the generation of the fiber structures with the passage of shock fronts through narrow jets in the wake of Coronal Mass Ejections (CME). Therefore the most probable emission mechanism of fibers in IP type II bursts appears to be resonance transition radiation (RTR) of fast particles at the boundary of two media with different refractive indices. The same mechanism is also valid for striae in the type III bursts. Taking into account a high-density contrast in the CME wake and the actually observed small-scale inhomogeneities, the effectiveness of the RTR mechanism in IP space must be considerably higher than in the meter or decimeter wavelengths. For the most part the fibers in the type IV continuum at frequencies of 14 – 8 MHz were seen as the direct expansion of similar fine structure (as fibers or "herringbone" structure) in the decametric range observed with the Nançay and IZMIRAN spectrographs.

Keywords Sun · Flare · Radio emission · Fine structure

G.P. Chernov (✉) · V.V. Fomichev · R.V. Gorgutsa
IZMIRAN, Troitsk, Moscow Region, 142190, Russia
e-mail: gchernov@izmiran.rssi.ru

M.L. Kaiser
NASA/GSFC, Greenbelt, MD 20771, USA

J.-L. Bougeret
Observatoire de Paris, CNRS, LESIA, 92195 Meudon, France

1. Introduction

The fine structure of radio emission in the form of the more or less regular stripes of emission and absorption, called zebra-pattern (ZP) or fiber bursts, with an intermediate frequency drift (IDB) as opposed to the continuum emission of type IV radio outbursts at meter or decimeter wavelengths, is well known in the literature beginning with the first report of Elgaroy (1959). They were classified and studied more than 25 years ago (Kuijpers, 1975a; Kruger, 1979; Slottje, 1981).

The observations with *WIND/WAVES* receiver (1 – 14 MHz) also show fine structure in interplanetary (IP) radio bursts (Bougeret et al., 1995). Flocculent (wisp or patch) structure in II type bursts and rapid pulsations in IV type continuum are frequently present (see http://lep694.gsfc.nasa.gov/waves/waves.html). There also exist shock-associated (SA) events in the decametric (DCM) range as the extension into IP bursts of "herringbone structure," which are generally considered as evidence of shock acceleration (Bougeret et al., 1998). In addition, different fiber-like structures are sometimes observed in conjunction with type II or type IV IP bursts. The object of this paper is to study similar fiber structures in relation to ZP and IDB in the metric ranges.

Results of observations, combining the *WIND/WAVES* data with spectra in the metric range (Nançay and IZMIRAN) and other data (SOHO LASCO and EIT images) are described in Section 2. Verification of the existing theoretical mechanisms is carried out in Section 3.

2. Observations

2.1. General Descriptions of Events

In this section, examples of the basic forms of fiber structures in spectra from *WIND/WAVES* RAD2 are presented, and all of the possible associated phenomena are briefly described. Primary attention will be paid to the examination of type II bursts and CME. In Figures 1, 2, 4, 6, and 8 – 14 the basic examples of typical spectra with fiber structure of the interplanetary (IP) type II + IV bursts are given. All of the main properties of the selected 14 events are summarized in Table 1. In the latter four columns the spectral parameters of the fiber structure are collected: Δf, the total frequency band, encompassed by structure; Δf_e, the frequency bandwidth of isolated fiber in emission; Δf_s, the frequency separation between adjacent fibers; and $\mathrm{d}f/\mathrm{d}t$, the frequency drift of the fibers. In the fourth column, in addition to the speed, the abbreviation of the observatory where the dynamic spectrum of type II meter burst was observed is also noted.

The events of 2 May 1998, 17 September 2001, and 3 November 2003 will be examined in more detail, since in these events the extension of the metric type II bursts (or type IV continuum) into IP bursts was observed, and the richest data in other ranges are assembled.

Some conclusions from Table 1

The fiber fine structure is a rather rare event among numerous IP bursts, but not less rare than analogous structure in the meter wave band. Statistics will be inaccurate, if we will attempt to determine it.

Of the 14 selected events, seven exhibit the fiber structure in type II bursts, five in type IV continuum bursts, and two — as striae — in type III bursts. The clear, reliable continuation of meter type II burst into IP type II burst was observed only in the events of 2 May

Table 1 Selected fiber patterns in IP radio bursts with *WIND/WAVE* RAD2 spectra.

Date UT	Dur min	Flare, coord.	Type II V km s^{-1}	CME V km s^{-1}	Δf MHz	Δf_e kHz	Δf_s kHz	$\mathrm{d}f/\mathrm{d}t$ kHz s^{-1} Type
12 Dec 97	30	B9.4	1 000	LE loop	1 – 5	200	400	−1.8
22:30		N25W52	Hir	207				IV fibers
02 May 98	130	X1.1	960 N	Halo	1 – 6	200 – 300	>500	< −2.78
14:10		S15W15	400 N	1 040				II fibers
18 Apr 00	68	No data	?	No	1.5 – 4	100	>200	−0.69
22:10		N17E90	Wind					II fibers
		EIT195	IP630					
19 Apr 00	210	C1.2	?	No	1 – 2	105	>300	−0.40
01:30		N19E73						II fibers
17 Sep 01	32	M1.5	685	P. Halo	5 – 14	500 – 700	>1 200	−8.33
08:30		S14E04	5 540	1 000				II + IV
			Izmi	1 400				fibers
20 Jul 02	30	X3.3	600	OA Halo	7 – 14	1 000	>1 500	−8.93
21:30		SE limb	Culg	1 941				IV fibers
27 Oct 02	20	C4.3	900	OA Halo	6 – 14	1 000	>3 000	−22.2
23:10		?N24W42	Culg	2 115				IV fibers
03 Nov 03	15	X2.7	705	W65	1.3 – 3.2	150	>300	−0.926
01:12		N10W83	Hir	827				III striae
03 Nov 03	30	X3.9	1 700	W103	6 – 14	800	>1 000	−12.35
10:10		N08W77	Izmi	1 420				IV fibers
							200	Type II
13 Nov 03	18	M1.4	714	P. Halo	6 – 14	150 – 200	>300	−4.29
09:30		E limb	Izmi	1 141			Rope	II fibers
			Ip 1 500					
18 Nov 03	>84	M4.5	4 000	P. Halo	2 – 4.5	200	300	−1.85
10:10		S04E16	800	1 824				II fibers
			Ip 656					
13 Jul 05	57	M5.0	457	Halo	1.6 – 14	300 – 1 000	Isol.	−16.7
14:08		N11W90	Nan	1 423			fibers	−2.08
			Ip ?					
23 Aug 05	36	M2.7	SAG	P. Halo	8 – 14	1 000	>1 500	−11.1
14:42		S14W90	IP 738	2 090				II + IV
								fibers
31 Aug 05	20	C2.0	?680N	Halo	1 – 14	100	200	−0.79
11:40		N13W13	IP III	860				III striae

1998 and 3 November 2003 (10:00 UT, together with the type IV continuum) in agreement with the results of Cane and Erickson (2005) about the rarity of such events. In four events (17 September 2001, 27 October 2002, 13 November 2003, and 13 July 2005) we see only the continuation of the continuum emission with fiber structure mainly at frequencies 14 – 5 MHz. Possibly, the same continuation was observed during the event of 23 August

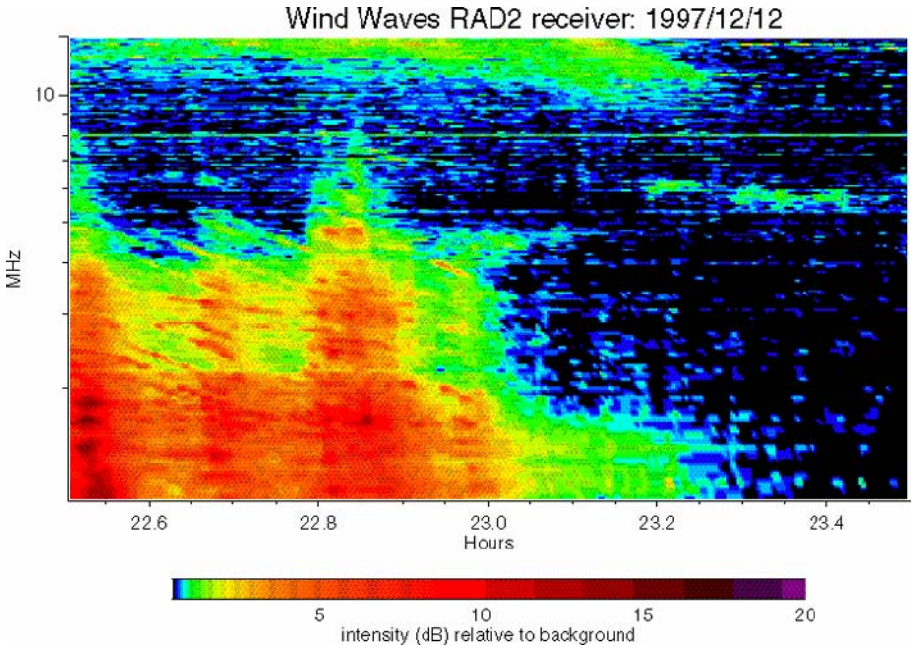

Figure 1 Multiple fibers and striae similar to zebra pattern in a type IV continuum burst.

2005, but the spectrum of the type II burst is absent, although the motions of sources at 164 MHz were observed with the Nançay Radioheliograph.

2.1.1. 12 December 1997 Event

The event was rare according to all of its properties. First of all, the continuum is located separately from DCM spectrum (Figure 1), but in the same continuum it is possible to distinguish type III bursts, consisting of striae. According to Hiraiso data, the metric radio burst was very weak: there are continuum with type III bursts and fairly present type II burst. The corresponding CME was very slow (207 $\mathrm{km\,s^{-1}}$) and showed streamer structure. The IP burst is not an extension of metric activity. But if we assume these striae to be ZP, then the relative values of the parameters ($\Delta f_e/f \approx 0.067$ and $\Delta f_s/f \approx 0.14$) exceed by more than an order of magnitude the analogous values for ZP in the meter range.

2.1.2. 2 May 1998 Event (Observations)

This is one of the most interesting events, because both in meter and decameter ranges two type II bursts were observed, and in both ranges the fiber structure was also recorded. In this connection, this event can be a key for understanding of the generation mechanism of this structure. Two type II bursts with fiber structure observed by *WIND* RAD2 receiver in the frequency range $\Delta f \sim 1-6$ MHz are shown in Figure 2. However, it is difficult to distinguish fiber structure at frequencies 14 – 6 MHz. Strictly parallel stripes in the type IV continuum (similar to the zebra) are caused by spin modulation of the spacecraft (the spin rate is about 20 per minute).

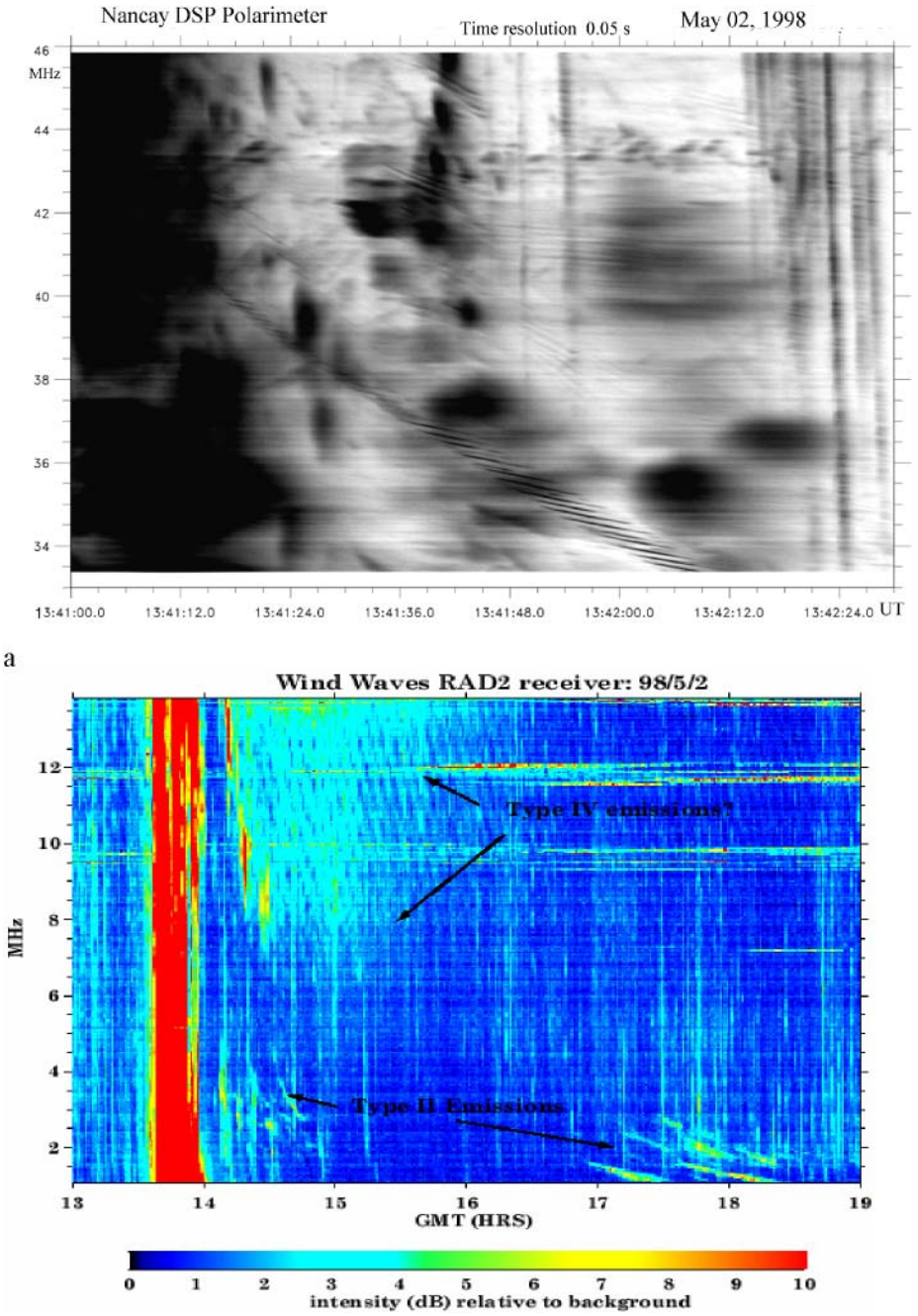

Figure 2 (a) Dynamical spectrum obtained by the decameter spectropolarimeter (DSP) of the Nançay Observatory. (b) Two IP type II bursts consisting of narrowband fibers. Strictly straight stripes in the continuum are caused by an artifact arising from the spin modulation of the spacecraft.

The absence of spin modulation in type II and III bursts could be explained by their weak polarization, since this modulation arises only with two perpendicular X,Y-antennas (Reiner et al., 2006). In such a case, the type IV continuum was strongly polarized. In this event we see the fiber structure of the type II bursts with large diversity in the frequency separation between the fibers. Thus, here no similarity with the ZP is observed. The frequency drift of separate fibers is approximately equal to the drift of the type II burst as a whole. To study this event in more detail, let us examine parameters of the fiber structure in the meter wave range.

ZP and fibers in the meter wave range

The radio event of 2 May 1998 was connected with a large 3B X1.1 flare at 13:30 – 13:42 – 15:13 UT in the active region NOAA 8210, with coordinates S15W15. The SOHO/LASCO telescope detected a major halo-type coronal mass ejection (CME) extending to 26 $R_{\odot}$.

The radio event included a large group of type III bursts, two type II bursts, and type IV continuum radiation. A global dynamical spectrum is presented by Leblanc et al. (2000). The maximum radio flux was observed at decimeter wavelengths (22 000 s.f.u. at 606 MHz), but the event extended to lower frequencies as type II and III radio bursts. ZP structures were first observed at frequencies between 22 – 46 MHz (Nançay DCM spectrometer-polarimeter) against the flare continuum after the strong type II and type III bursts (Figure 2), its duration being more than three minutes.

The dynamical spectrum in the upper panel of Figure 2 shows that the zebra structure consists of numerous fragments of stripes with various frequency drifts. The most evident long fragment resembles a narrowband rope of fibers with a constant frequency drift. This main rope of fibers, with the duration of about two minutes, forms the low-frequency boundary of all the zebra-pattern fragments, some of them also forming ropes of fibers at higher frequencies. The frequency drift of the main rope is approximately -0.13 MHz s^{-1} near 35 MHz. The frequency drift of separate fibers is much less, ~ -0.04 MHz s^{-1}. We should note two more important properties of the main rope: its frequency width increased from 0.25 MHz at 43 MHz to 0.8 MHz at 22 MHz, but the degree of left-circular polarization appreciably decreased.

The width of the frequency bands for individual stripes of emission was approximately the same for all the zebra-structure fragments, $\Delta f_e \approx 0.08$ MHz, with the relative width of these bands being $\Delta f_e/f \approx 0.0024$. However, the frequency separations between the stripes of emission were appreciably different in different fragments ($\Delta f_s \approx 0.08 - 0.17$ MHz), and the main ropes are not strictly periodic in frequency. In some fragments, a low-frequency absorption is observed, and frequency separation between an emission stripe and the neighboring absorption, Δf_{ea} is approximately equal to Δf_e. The radio emission of all the components of the type II and type III bursts was essentially unpolarized, while the main rope displayed strong left-circular polarization (black in the spectrum in Figure 3). Other fragments of the zebra structure displayed moderate right-circular polarization (white in Figure 3). Two-dimensional NRH radio source images at 164 MHz show four radio sources above the active region NOAA 8210. The complex behavior of the polarization of the fine structure may indicate that different radio sources are located in regions with different magnetic polarities.

The lower part of Figure 3 displays the evolution of the flare in the 195 Å EUV line (five frames from SOHO/EIT sequence), while the sixth lower panel shows the onset of the Hα flare. We can see in this last panel that a helmet-like ejection has already formed above the sigmoid flare ribbon by 13:24 UT. The continuation of this ejection is clearly visible in the

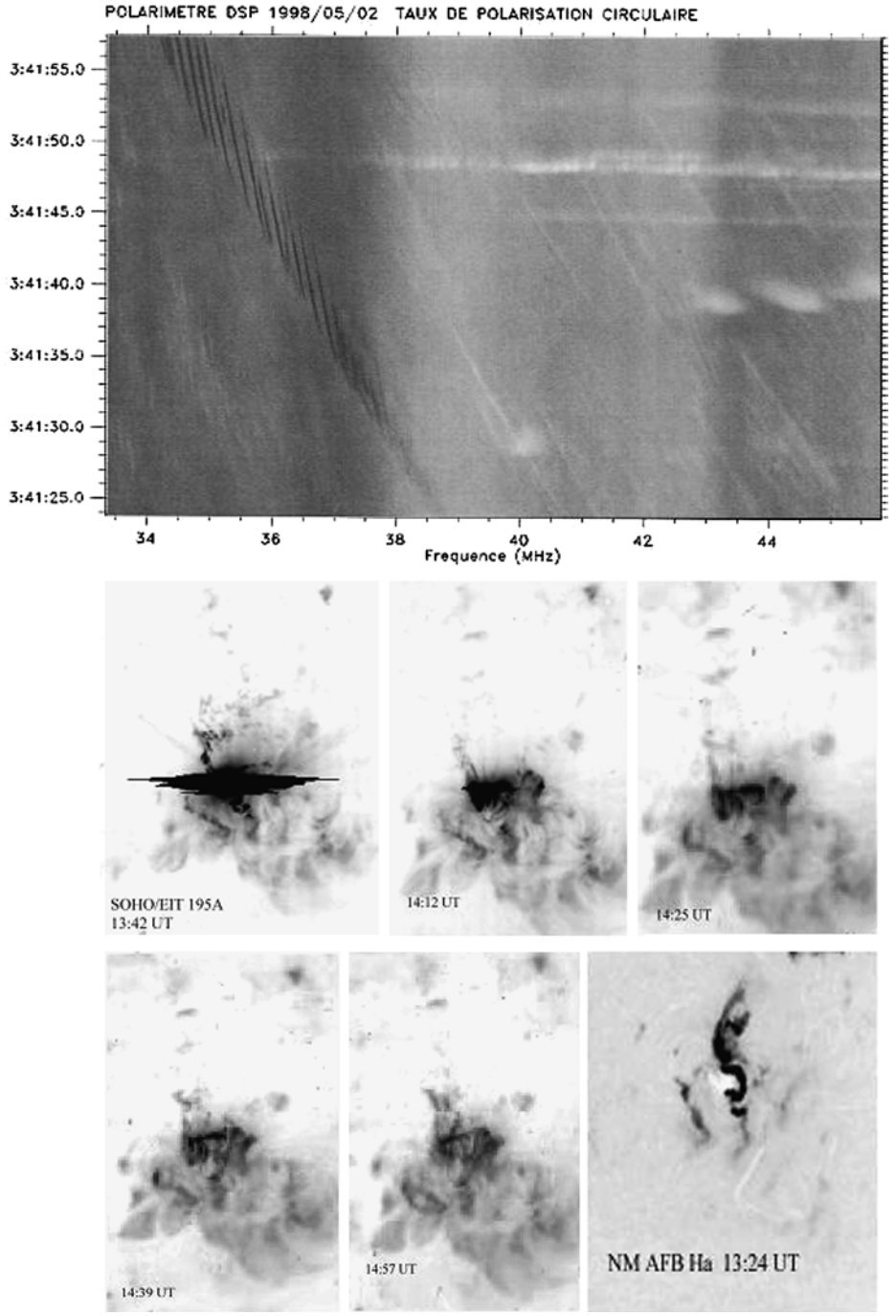

Figure 3 Event of 2 May 1998. The top panel shows the degree of circular polarization in the dynamical spectrum obtained using the decameter spectropolarimeter (DSP) of the Nançay Observatory (the time resolution is 0.05 seconds). The lower panels show the development of the outburst in the 195 Å EUV line (SOHO/EIT) and the Hα emission in the Active Region 8210.

first 195 Å frame, which corresponds to the maximum of the flare (13:42 UT). We can see also two ejections, northwards and southeastwards. Taking into account the presence of the two type II bursts, it is probable that the upper ejection caused the first type II burst, and the lower ejection caused the second such burst. Each subsequent frame contains new fragments of ejected material in projection on the disk.

According to the Nançay spectra, the first type II burst began at 70 MHz at ∼13:40 UT and the second one ∼13:48 UT. The frequency drift of the first burst was ~ -0.143 MHz s^{-1} which corresponded to the velocity of the shock front ∼960 km s^{-1} using the density model of Leblanc, Dulk, and Bougeret (1998). The velocity of the second shock was much less, ∼380 km s^{-1} (Leblanc et al., 2000). This latter corresponds to the slower movement of the ejection in the southeast direction in the subsequent pictures in Figure 3.

The CME appeared at the height of 2.0 $R_\odot$ at 14:06 UT. Taking into account the CME velocity of 1040 km s^{-1} it is easy to show (using the height-time diagram), that the CME has arisen high in the corona, at any rate, near a plasma level of 80 MHz ($\sim 1.0\,R_\odot$). Thus both shock fronts were blasts without any relation to the CME. The rope fiber structures were observed during the first type II burst just at the flare maximum. Behind this first shock front, the second slow shock front propagated, and ahead of it was the CME with greater velocity than that of the first shock front. Two type II bursts appeared at 14 MHz (*WIND* RAD2 spectrum in Figure 2) approximately at 13:45 and 14:07 UT (the beginning of the first one coincides with the powerful type III bursts). The delay between them increased from 8 minutes at 70 MHz to 13 minutes at 14 MHz, which is related to the smaller velocity of the second shock front. It is obvious that after the CME, the energy release occurred in a vertical current sheet which had a magnetic structure with magnetic islands. Therefore the appearance of ZP in the decimeter range at 14:29 UT (shown in Jiřička et al., 2001) at post-flare phase can be correlated with such magnetic islands.

The appearance of a fiber structure in IP type II bursts is probably connected with the passage of the shock front through a jet structure behind CME. We see such narrow streamers in the LASCO C2 image exactly at 15:03 UT (see Section 2.1.6) at the heights $\sim 3\,R_\odot$, corresponding to plasma frequency of 4 MHz (according the model of Leblanc, Dulk, and Bougeret, 1998). In the range 1 – 5 MHz, the relative values of the parameters of fibers are greater by approximately an order of magnitude than in the metric range.

Discussion of the 2 May 1998 event

The rope of fibers shown in Figure 2 strongly resembles similar structures observed earlier at higher frequencies (200 – 250 MHz) which were discussed in Mann et al. (1989) and Chernov (1997). However, these latter structures were repeated multiple times during the entire decay phase of the flare (more than an hour). They are associated with whistler instabilities in a small magnetic trap which has been formed between shock fronts moving away from a magnetic reconnection X-point during the prolonged process reestablishing the magnetic structure after the CME.

In Figure 3 we can see ejecta in various directions in five frames in the 195 Å line (SOHO/EIT), but two of them are most prominent: one northward from the main flare and the other southeastward (a slowly-moving front). According to the first EIT 195 Å image (13:42 UT), it is possible to assume that the radio source of fine structure was located in a turbulent zone between two shock fronts. The different polarization signs of the main rope of fibers and surrounding its zebra structure (shown in Figure 3 in the top spectrum in circular polarization) testify to the presence within the source of different magnetic polarities. Most likely, this source is an X-region of magnetic reconnection.

Thus, it is most probable that the source of the fiber rope is associated with the turbulent zone behind the fast shock front and is located in a narrow trap between the fast front and the slow front. The ropes are observed for only three minutes during the type II burst, and the frequency drift of the main rope is determined by the motion of the shock front with a speed of $\approx$960 km s^{-1}, because the frequency drift of the main rope is almost equal to the drift of the fast front.

Fast particles accelerated in the shock front were captured in this narrow trap. According to the dynamic spectra at the moment of the beginning of the second type II burst at 70 MHz, the first burst was located approximately at 20 MHz. Using the density model of Leblanc, Dulk, and Bougeret (1998), we estimate the distance between the shock fronts at this moment approximately as 300 000 km. Trapped fast particles with the typical velocity for the type III bursts of order 10^{10} cm s^{-1} pass this distance for three seconds. Specifically, this is the average period between the separate fibers in composition of rope. As a result of the "bounce" effect, or the motion of these particles between the two maxima of the magnetic field (between two shock fronts), a loss-cone velocity distribution was formed, giving rise to a periodic whistler instability. The increase of the distance between the two shock fronts can explain the smooth expansion of the main rope during the drift toward lower frequencies. In general, the shock front probably propagates at some angle to the magnetic field. In this case the magnetic field and density of the shock front should have an oscillatory structure. Such a structure may explain the origin of a number of other fragments of fiber ropes and zebra stripes at higher frequencies, whose sources are located further behind the fast shock front.

The whistlers propagate in the direction of propagation of the shock front. It is natural to assume that whistlers are excited before the shock front (where the background plasma has the ratio of cyclotron and plasma frequencies $(f_{Be}/f_P) = 1/30$ and the relative whistler frequency $(x = f_w/f_{Be}) = 0.01$. The magnetic field varies little (according to the constant parameters of narrow fibers), but whistlers scatter on the background plasma, resulting in a sharp reduction of x (Chernov, 1989). Besides, the presence of the broadband main rope means the presence of a density heterogeneity with increased plasma density (two to three times). Therefore the group velocity of the whistlers

$$v_{\rm gr} = 2c(f_{Be}/f_{Pe})\left[x(1-x)^3\right]^{1/2} \tag{1}$$

(Kuijpers, 1975a) should be noticeably less than 10^8 cm s^{-1} (*e.g.* for $f_{Be}/f_{Pe} = 1/45$ and $x = 0.0033$, $v_{\rm gr} = 760$ km s^{-1}), providing an explanation for the appreciably lower frequency drift of the fibers within the main rope in the comparison with the drift of the rope (whistlers lagged behind the shock front). Thus, these unusual fiber ropes are most likely a manifestation of whistler wave packets propagating between two shock fronts in the corona. The short total duration of each fiber (gradually growing from approximately two seconds at 38 MHz to seven seconds at 35 MHz) is determined not simply by the growing interval between the fronts, but most likely by cutting emission as a result of the cyclotron damping of whistlers with the decrease of the field strength and reaching $x = 0.5$. It is evident from Figure 3 that the shock fronts propagated at different angles, therefore it is possible to assume that fibers and ZP were observed only in the time interval, thus far the fronts overlapped in space, that is below approximately 20 MHz (above 1.6 $R_\odot$). At lower frequencies of 14 – 8 MHz the type II bursts have only the usual flocculent structure.

2.1.3. 17 September 2001 Event (Observations)

The IP burst, shown in Figure 4c, presents fiber structure as it expands from the metric range (may be of type II burst and group of strong type III bursts), containing strange fragments

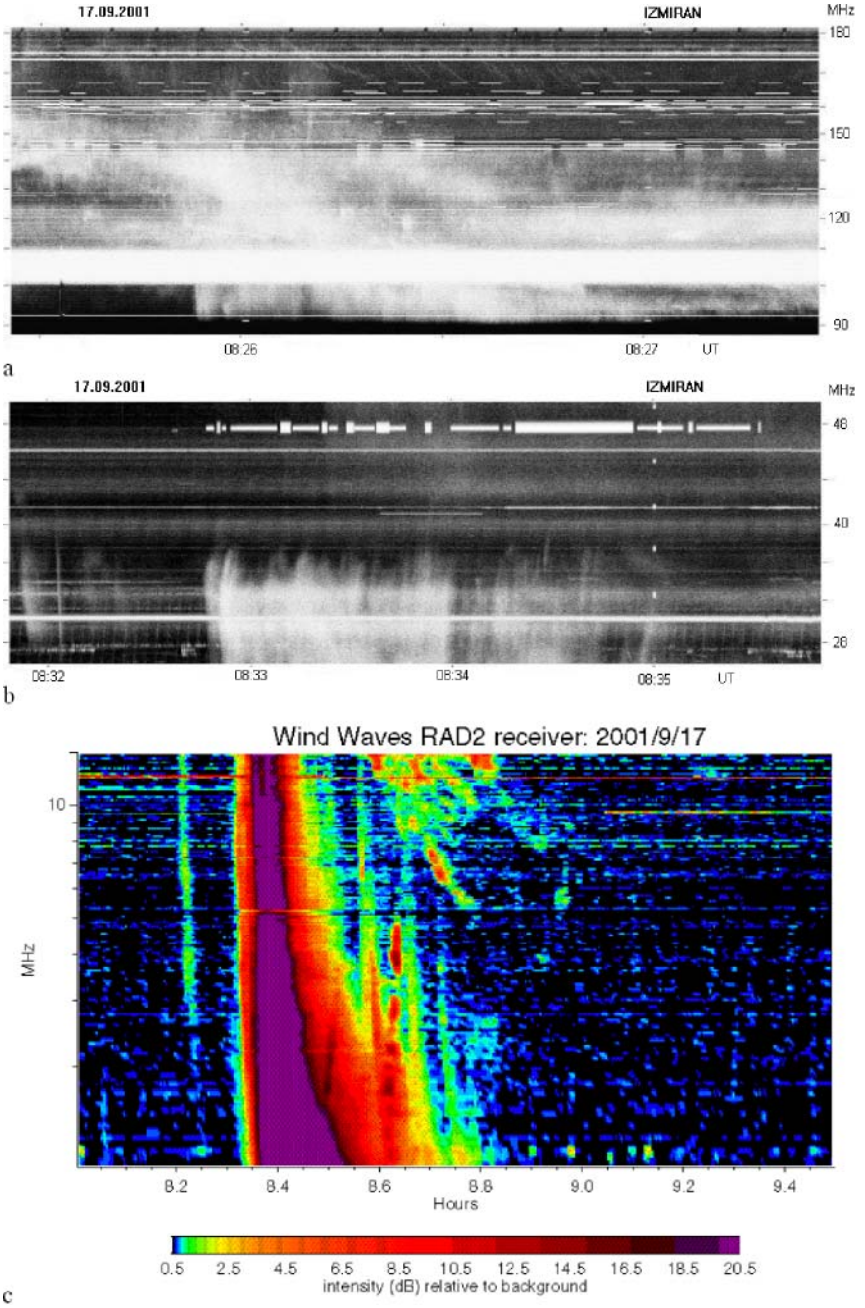

Figure 4 Increased fragments of the metric spectrum (IZMIRAN) show numerous narrow frequency fibers between 190 – 175 MHz (a) and the herringbone structure at the low frequency part of the fundamental band of the slow type II burst (b). (c) Multiple fibers as extensions of the metric type II bursts into the RAD2 spectrum. After strong type III bursts, two fragments with reverse frequency drift, like type U-bursts, are also visible between 1.6 and 4.6 MHz.

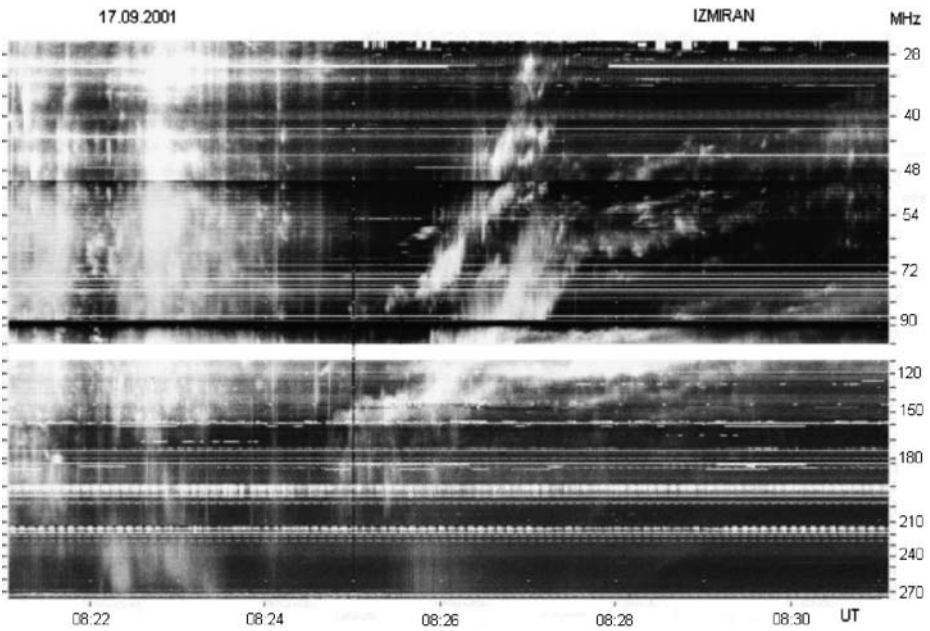

Figure 5 The general view of the dynamical spectrum in the metric range (IZMIRAN) of the 17 September 2001 event, demonstrating strong type III bursts in the beginning and two type II bursts with harmonic bands.

of reverse drift bursts (similar to U bursts). In the metric range, the radio event consisting of strong type III bursts and two type II bursts (Figure 5) began simultaneously with the M1.5/2N flare on 08:20 UT in Active Region 9616 with coordinates S14E04. Both type II bursts began almost simultaneously at 08:24:50 UT and consisted of fundamental and harmonic bands, but they drifted with sharply different drift velocities: the first slow burst (but prolonged),with $\mathrm{d}f/\mathrm{d}t \approx -0.135$ MHz s^{-1}, reached the frequency of 25 MHz at 08:33 UT; the second (rapid) burst ended at 25 MHz approximately at 08:27 UT and had a drift velocity almost five times greater than the slow one.

The analysis of SOHO/EIT images in the 195 Å line shows two ejecta at 08:24 UT which propagated at different angles and were visible until 08:36 UT. At the same time interval, the two-dimensional maps of the Nançay radioheliograph at 164 MHz show two radio sources approximately in these directions. So, two type II bursts could not be radiated by one shock front, *e.g.*, by different parts of this front with different density gradients. Unusually high frequency drift, -0.6 MHz s^{-1} is certainly connected to this effect.

The SOHO/LASCO data show the partial halo CME, and on the height-time diagram at the moment of type II burst beginning (08:25 UT) the CME was located at the height of 1.5 $R_{\odot}$ (or at the level of 25 MHz), *i.e.*, much higher in the corona.

In Figures 4a and b the increased fragments of the metric spectrum are shown. The first spectrum presents numerous narrow frequency fibers between 190 – 175 MHz with some elements of rope similar to ropes discussed in Chernov (1997). The second spectrum shows the herringbone structure at the low-frequency part of the fundamental band of the slow type II burst, and this structure (between 08:33 – 08:49.5 UT) passes continuously into fibers in the range 14 – 5 MHz in the *WIND*/RAD2 spectrum. Some type III bursts are also observed in the IZMIRAN data.

Thus, some analogy is found with the event on 2 May 1998. Here fiber ropes and two type II bursts in the meter range as well as the expansion of one of them into the WIND spectrum as drifting fibers were also observed.

The clear difficulty for interpretation represents the transition of the herringbone structure with separate very-quickly drifting bursts (and with different sign) into slowly drifting fibers with the drift speed close to the usual drift of type II bursts.

2.1.4. 3 November 2003 Event (Observations)

The similar transition of fiber structure in the metric range into fibers in the WIND spectrum is shown in Figures 6a and b. The event was related to a large X3.9/2F flare in AR 0488 on the west part of the disc at N08W77. Taking into account all of the harmonic relations between the bands of complex type II bursts, shown in Figure 7, we are compelled to recognize the presence of two type II bursts. The low-frequency burst (140 – 40 MHz) with a frequency drift $\mathrm{d}f/\mathrm{d}t = -0.3$ MHz s^{-1} was obviously caused by another shock front judged by its complete stop (attenuation) at frequencies ∼40 MHz. The first type II burst with harmonic structure drift to 25 MHz (at 10:05 UT), though with a somewhat lower frequency drift. The velocities of the shocks estimated within the framework of the double Newkirk model are equal about 1770 km s^{-1} for the fast burst and about 1000 km s^{-1} for the slow one. Both shocks were of the blast type and were related to the eruptive phase of the flare. The CME began some minutes later and its velocity was 1420 km s^{-1}, thus both shock fronts were propagating far ahead of a CME. Although the fast type II burst stopped at 40 MHz, on the *WIND* spectrum we notice its continuation after 10:10 UT but with two strange harmonically related type U bursts (with turnover frequencies near 3 MHz and 6 MHz for the fundamental and harmonic respectively) and subsequent narrow stripes (or fibers also with harmonics) which appear as a continuation of falling branches of U bursts between 5 – 1.5 MHz in the interval 10:20 – 10:40 UT (Figure 6b). The velocity of IP front determined by the frequency drift of narrow fibers in the Leblanc, Dulk, and Bougeret (1998) model, is about 700 km s^{-1}, *i.e.*, the CME was overtaking it. Thus this strange IP burst could not be initiated by the forward edge of CME, as in this case the speeds of the CME and the shock front should be approximately equal.

The fibers in the 90 – 30 MHz range against the background of wisp structure of the second type II burst (Figure 6a) are similar to fiber bursts (IDB). However the speed of the frequency drift is about equal to or less than the drift speed of the type II bursts, and they cannot be classified as fiber bursts (IDB). They also cannot be identified with ropes (Chernov, 1997) because they are larger-scale. As always, in each event fibers in type II bursts are varied and depend on the shock front structure. It is possible to say quite definitely that their source was located between two shock fronts.

Comparing this event with the two previous ones, we nevertheless notice the clear analogy in the origin of the fine structure in *WIND* spectra. But first of all we should note that the continuum emission in the *WIND* spectrum (14 – 5 MHz) is a direct expansion of flare continuum from the meter range, and the fibers are direct continuation of those of the meter range. The fibers are formed as a result of the interaction of plasma waves with whistlers, generating and propagating inside a magnetic trap, in this case between two shock fronts.

We assume that the CME overtook the slow front at around 10:02 UT, at the beginning of the ascending branches of the U bursts. This assumption, on the whole, is supported in the recent paper Vrsnak et al. (2006), where the diagram of this overtaking is shown in Figure 5. A mismatch in the time is certainly present, with the trajectories of CME and slow

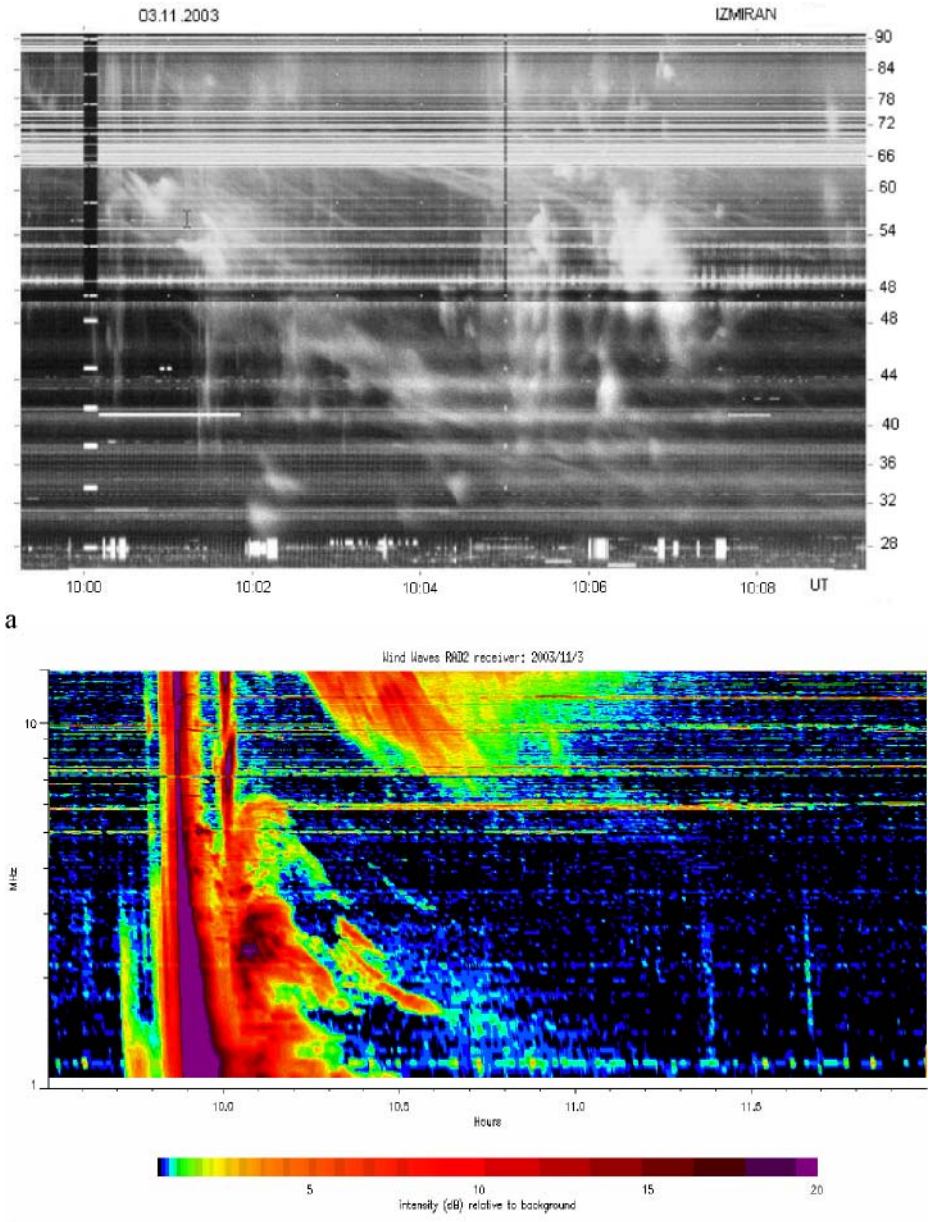

Figure 6 The continuation of fiber structure from the DCM range in the continuum emission and fragments of type U burst and fibers in type II burst at low frequency part of the RAD2 spectrum.

front intersecting approximately at 10:15 UT, but it is difficult to expect an ideal agreement using different density models.

Unusual U bursts in the *WIND* spectrum testify to the clear closed magnetic configuration at heights $2-4\ R_{\odot}$ (a magnetic cloud) that specifies a capture of fast particles in this interval

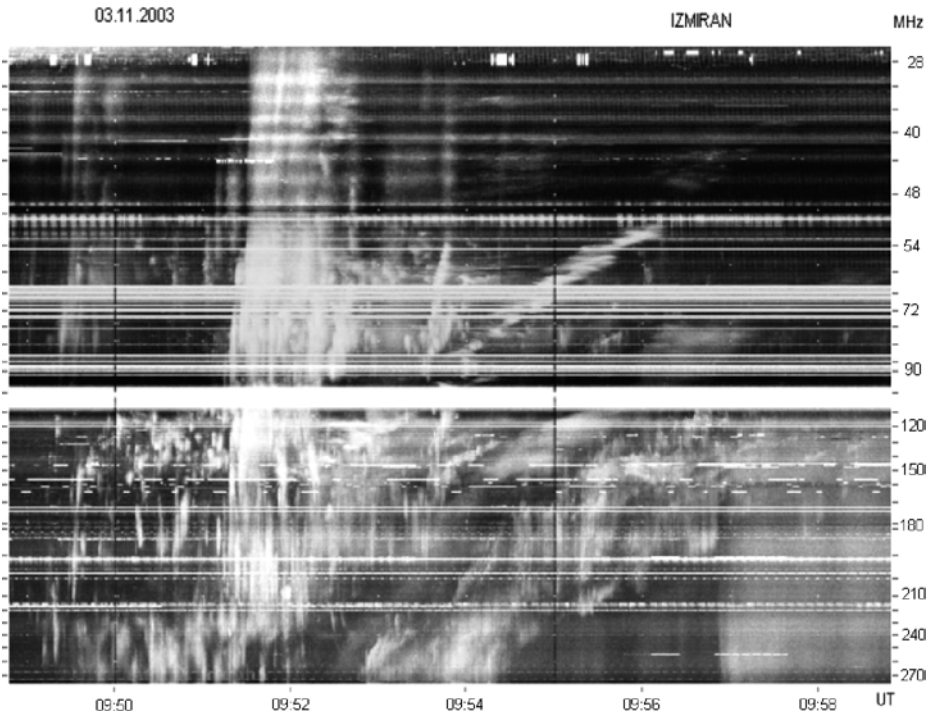

Figure 7 The general view of the dynamical spectrum in the metric range of 3 November 2003 event, demonstrating strong type III bursts in the beginning and two type II bursts with harmonic bands.

of heights between shock front of the IP burst and the forward edge of the CME. Recall that this IP shock front lagged behind the CME. Therefore the generation of narrowband fibers in the IP takes place in elongated density heterogeneities in the wake after CME passage, clearly visible on the SOHO/LASCO image. Moreover, in the left bottom image at 10:32 UT a diffuse emission strip behind the forward edge of CME (marked by the arrow in Figure 11) is probably the manifestation of the shock front against the background of the CME wake.

2.1.5. 13 November 2003 Event (Observations)

The main peculiarity of this event is an occurrence of structure such as the rope in the IP burst (Figure 8b). In contrast to all other events, this one was connected with the flare on the east limb in AR 0501 of importance M1.4. The CME began almost simultaneously with the type II burst in the metric range about 09:26 UT. Most likely the CME and shock front were independent as the velocity of the CME was much higher (1140 km s^{-1}) than that of the shock front ($\sim$700 km s^{-1}). Therefore all of the fine structure was connected with a source between the forward edge of the CME and the shock front going behind it. We see in Figure 8a only the part of the herringbone structure drifting to high frequencies. The low-frequency part of this herringbone structure with opposite frequency drift is also seen in the *WIND* spectrum at the same time. The fast particles responsible for the herringbone structure could be then trapped between the forward edge of CME and the shock front, and we see only some manifestations of their possible bounce motions with the generation of plasma waves and whistlers. So, the mechanism should be

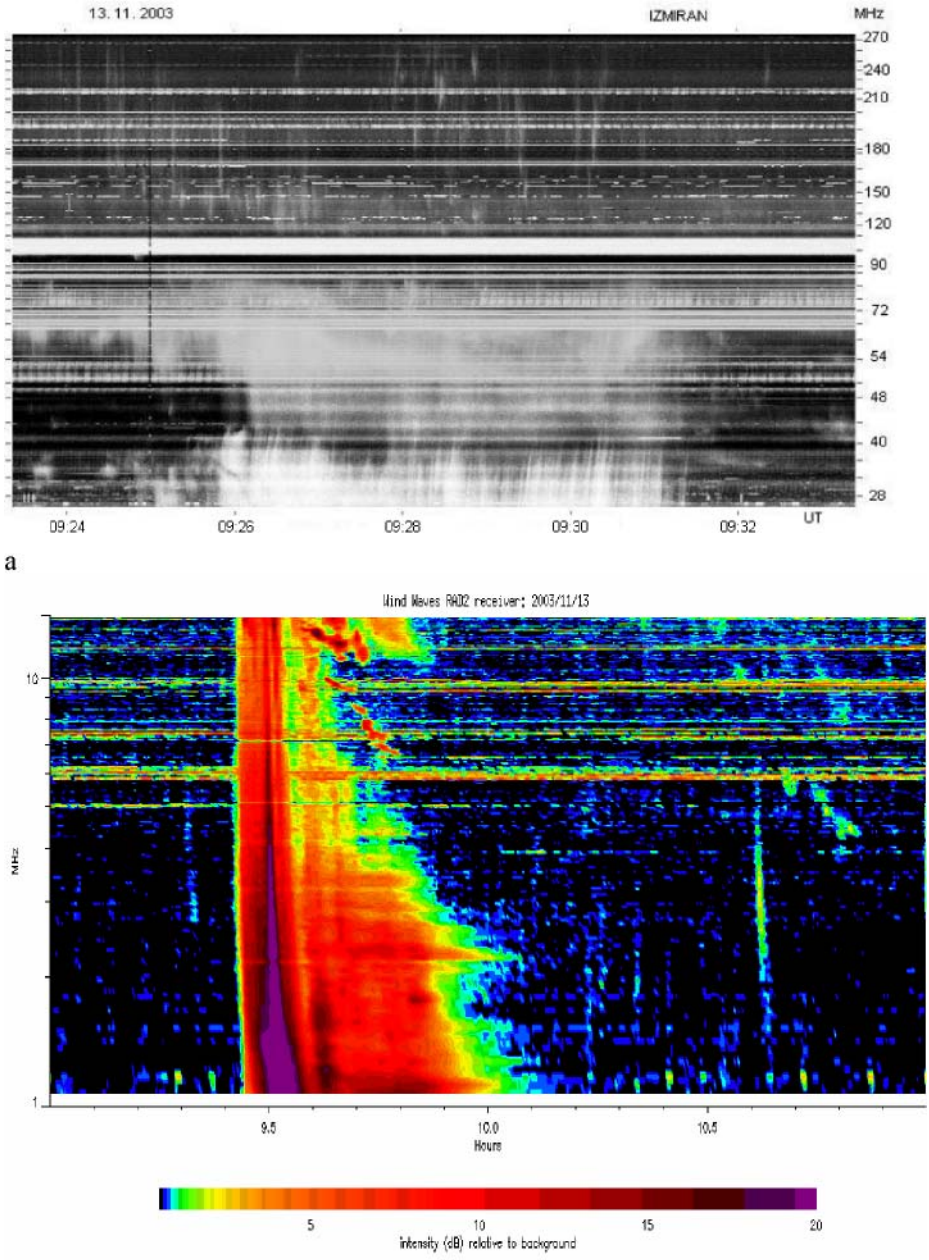

Figure 8 Herringbone structure in the metric type II burst (a), its expansion into RAD2 spectrum (b) but in another quality as some short slow drifting (-4.3 kHz s^{-1}) fibers forming a rope.

the same as for the fiber rope structure in the metric range, *e.g.*, discussed by Chernov (1997) and above in Section 2.1.2 (Discussion of the 2 May 1998 event), but at much

larger scales. The termination of radiation is not necessarily connected with a scattering or merging of fronts, it is more natural to assume an angular divergence CME and shock front.

Some stria structure in continuum emission after type III bursts below six MHz is similar to the stria structure in the 12 December 1997 event, although here any frequency drift of striae is absent.

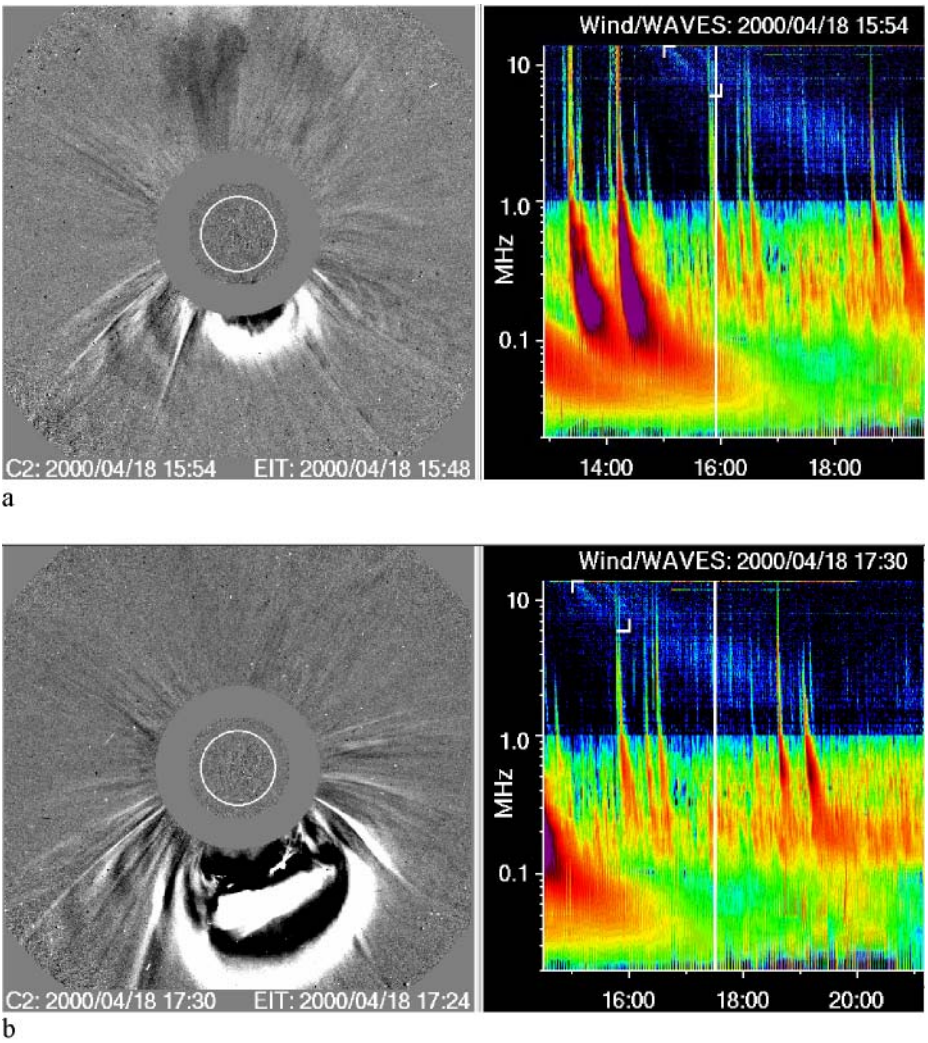

Figure 9 Two moments of combined LASCO C2 images and WAVE (RAD2+RAD1) spectra allowing the connection of the moment of radiation (marked by the straight vertical line on spectra) with a locating in the CME, as a source of radiation.

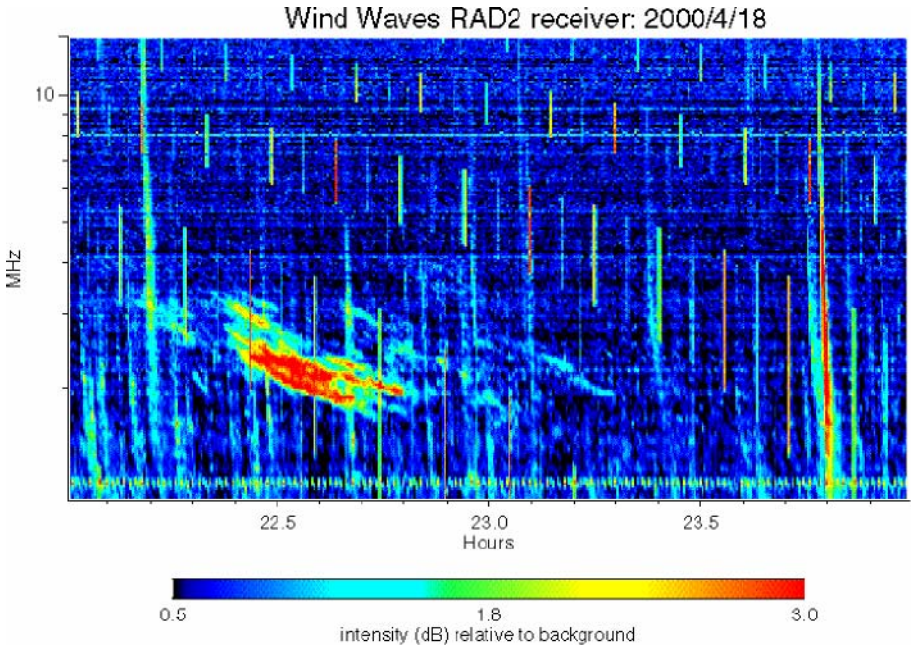

Figure 10 Multiple drifting fibers in a type II burst.

2.1.6. Other Events

For the 18 April 2000 event we have no information about flares and metric type II bursts. However, it is very interesting and consists of two bursts with fine structure (Figures 9 and 10). Despite numerous IP type III bursts, there are no bursts in the meter range in the spectrum from the Hiraiso observatory, and only a weak continuum present in the band 25 – 35 MHz in the interval 21:30 – 24:00 UT. Thus, it is obvious that the type III beams were accelerated at heights $\sim 2\, R_{\odot}$. At the same time, the first event (Figure 9) was accompanied by a powerful CME, and we have an opportunity to look for the CME site responsible for this radio burst. In the events discussed above, we followed only those heterogeneities in the shock front that propagated through after CME.

In the RAD2 spectrum a broadband drifting continuum is present, and against this continuum two drifting stripes are located in the high-frequency part of the spectrum. The common frequency drift of the continuum is somewhat less than the drift of fibers; it drifts through the whole range 14 – 1 MHz in approximately 80 minutes. In the model of Leblanc, Dulk, and Bougeret (1998) this drift corresponds to the speed 660 km s^{-1}, which practically coincides with the speed of the CME (668 km s^{-1}). In the absence of a type II burst (shock front), it specifies that the continuum is direct radiation in front of the CME. The structure of the CME (Figure 9b) does contain two fronts, therefore it is quite obvious that the first wide front is responsible for the radiation of the first broadband fiber, and the second one (narrow internal) for radiation of the second narrowband fiber. There is a break in the continuum emission between these fibers, which probably is connected with an area of rarefaction between the two fronts. A somewhat larger speed of the frequency drift of the fibers is determined by the large density gradients in the CME fronts. However, the disappearance of fibers at 16:00 UT remains to be explained because the structure of the CME with two fronts

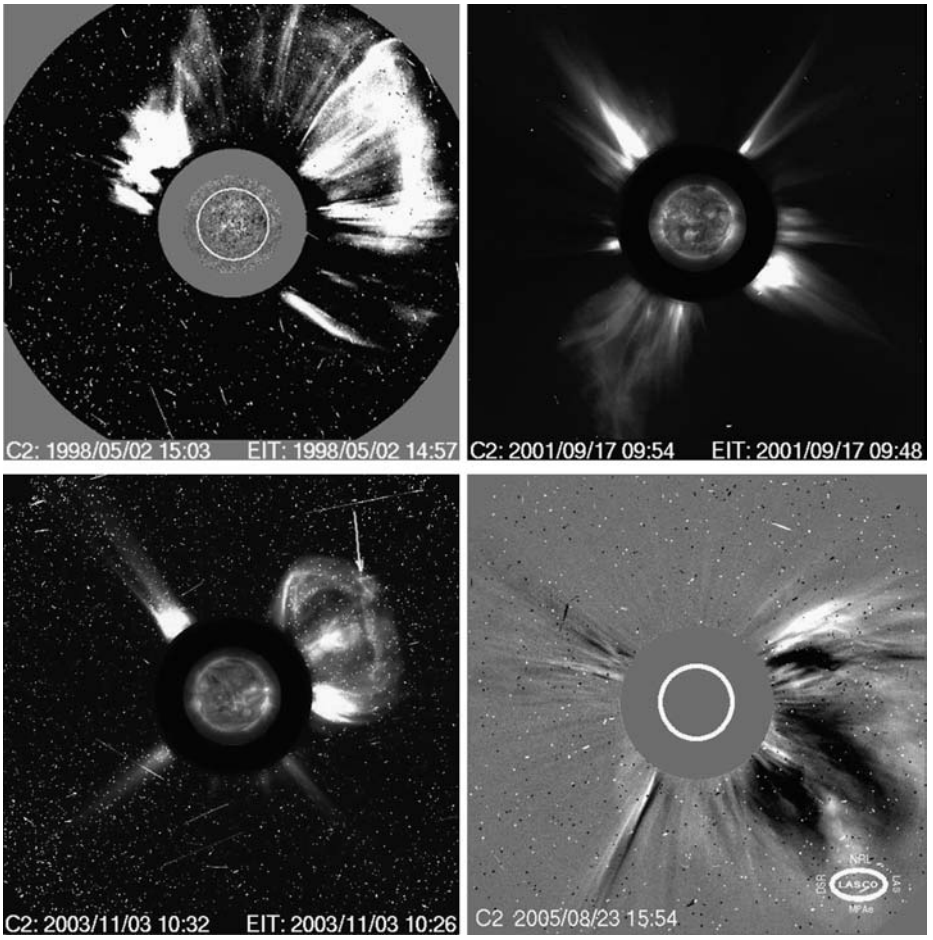

Figure 11 SOHO/LASCO C2 difference (2 May 1998 and 23 August 2005) and original (17 September 2001 and 3 March 2003) images with the streamer structure behind the CME leading edge. The CME on 3 November 2003 overtook the shock front, and the perspective position of the front is shown by an arrow.

remained long after 16:00 UT. The speed of the CME allows us to assume the occurrence of the shock front driven by the CME, then the rarefaction area is actually a reverse rarefaction shock wave. It is known that the speed of the reverse shock wave is less than that of the forward wave. The somewhat smaller drift velocity of the rarefaction area in comparison with the drift of fibers could be connected with that.

The second 18 April 2000 event at 22:30 UT is a typical IP type II burst in the range 4 – 1.5 MHz (Figure 10), and it is similar to the 2 May 1998 event. LASCO C2 images show a faint additional CME a little to the North of the previous one (not included in the catalog). It is possible that the shock front is also connected with this ejection. The IP space at the heights $2-5\,R_{\odot}$ remained perturbed after the previous CME passage, and the shock front radiated maximum emission from density enhancements similar to other events.

The 19 April 2000 event (Figure 12) is similar to the previous one. It presents a series of fibers repeating in time without a simultaneous CME. But during the day, type III noise bursts were observed and all strong bursts were accompanied by narrow ejecta in LASCO

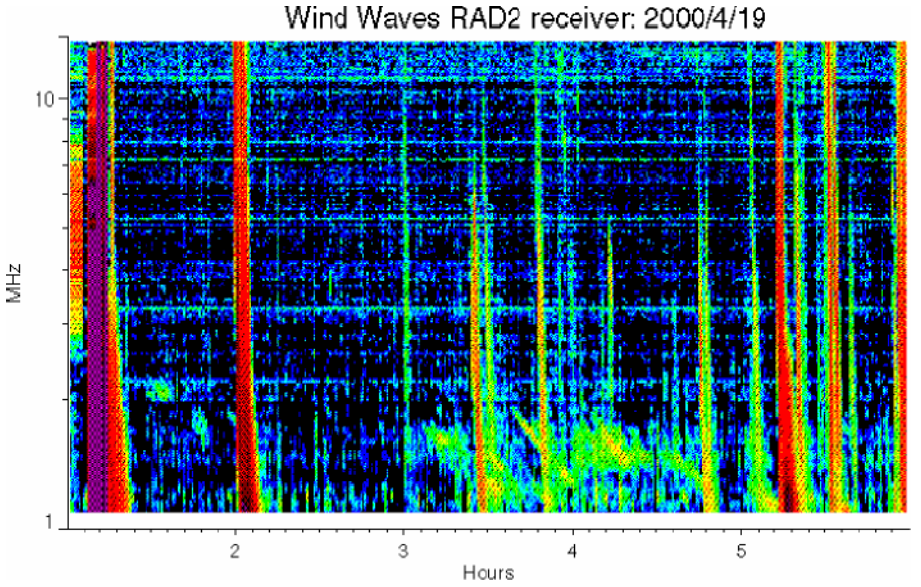

Figure 12 Multiple drifting fibers in a type II burst with a noise of type III bursts.

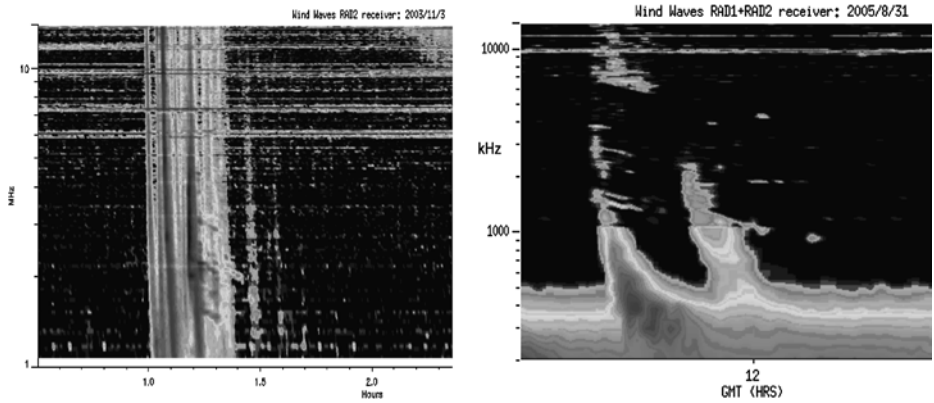

Figure 13 Two events with striae in the type III bursts.

C2 images, and the IP space was very structured. Taking into account some patch structure before fibers we can only propose the IP shock front propagating through these inhomogeneities. The fibers do not show strict periodicity and occupy different ranges of frequencies. In the 18 and 19 April events the general views of fibers are quite similar to fiber bursts (IDB) in the meter range.

Striae in type III bursts

In Figure 13, two groups (which may be unique) of type III bursts with striae are shown. Parameters of the events are shown in Table 1. It is evident that the striae occur only in the narrow zone of frequencies (heights). In contrast to striae in the meter range, here they

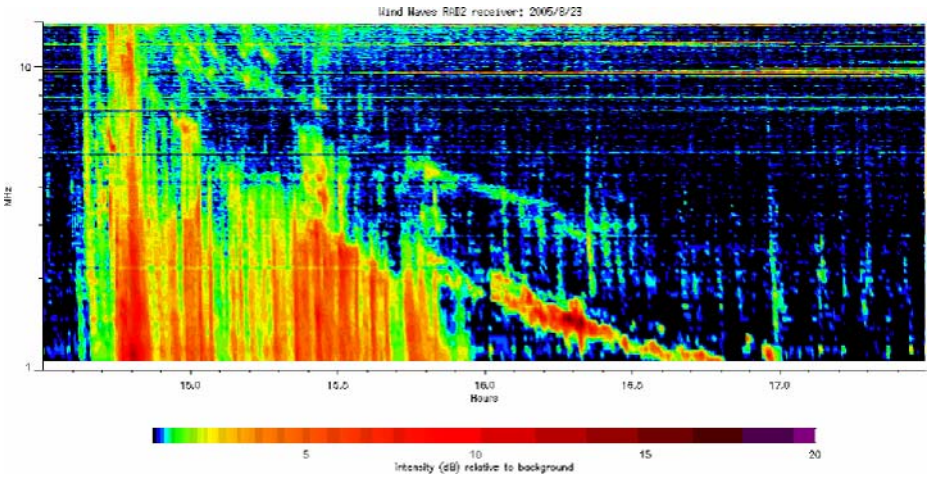

Figure 14 The 23 August 2005 event, showing the entire collection of fine structures: fiber structure in 14 – 7 MHz, two harmonic bands of type II bursts, and strong SA bursts.

drift to low frequencies, thus they almost do not differ from the fibers shown on Figure 12. Therefore their origins can be identical, with the only difference being that here the type III beams of fast particles meet a turbulent zone on the way. In the 19 April 2000 event the shock front crosses a similar zone, though it is clear that fast particles accelerated in the shock front are also responsible for formation of fibers.

The type III bursts are the most frequent phenomena in IP spectra, but such rare occurrences of stria structure could be explained by the fact that their major part usually is not connected with CME as well as with shock fronts, as happened in these two events.

The 23 August 2005 event (Figure 14) shows the entire collection of fine structure: fiber structure in 14 – 7 MHz, two harmonic bands of type II burst with a patch structure and strong SA bursts. But we have no spectra in the metric range. LASCO C2 images show streamer structure after the strong CME. This event was preceded by a radio source at 164 MHz moving to the West that was probably the source of the metric type II burst.

The 20 July and 27 October 2002 events are similar to the 17 September 2001 event. A direct expansion of the metric type II bursts (both observed by the Culgoora spectrograph) was manifested only as fibers at the high-frequency edge of the *WIND*/*RAD*2 spectrum. LASCO C2 images show the bright jet structure (narrow streamers) behind the CME front simultaneously with fibers and at the same heights (as well as in other events).

The 18 November 2003 event shows some peculiarity: after the strong metric type II burst, only some striae were observed at 08:30 UT, but after the second faint type II burst we see very marked fibers in IP type II bursts after 10:20 UT. A very marked jet structure after the partial halo CME remained at a distance 2 – 5 $R_{\odot}$.

The event of 13 July 2005 shows many isolated fibers in the whole RAD2 range after a strong drifting continuum in the metric range (Nançay DCM spectrum, 20 – 70 MHz). Some small scale jets remained 2 – 4 $R_{\odot}$ in the wake behind the halo-type CME.

3. General Discussion

First of all it should be noted that the time resolution of *WIND*/RAD2 spectra is limited by the time of one scan through 14 – 1 MHz, once each 16 seconds with an averaging time of one minute, and thus we can not distinguish all the fine structure elements as in the metric range with the IZMIRAN and Nançay spectrographs with the time resolution 0.04 – 0.05 seconds. So, the *WIND/WAVES* receiver can record only large features or sets of fibers. It is still necessary to specify in each event that the fibers have the peculiarities in all parameters (drift, frequency range, duration of separate fibers). Only the instantaneous frequency bandwidth is stable, 200 – 300 kHz for slow-drifting fibers in the type II burst, and 700 – 1000 kHz for fast-drifting fibers in the type II + IV (continuum). In addition, we have not found in IP bursts periodic and parallel-drifting fibers typical for meter and decimeter wave ranges, nor is there the classical zebra pattern with variable frequency drift of stripes. Only in the first event (Figure 1) are the stripes remotely similar to the zebra pattern. As a rule, the relative fiber parameters ($\Delta f_e/f$, $\Delta f_s/f$) exceed by an order of magnitude those in the meter range.

It is important to note that in practically all of the events with the expressed fine structure (as fibers), shock fronts of IP type II bursts went behind the leading edge of CME. In all the events, a certain connection between the occurrence of fibers and the presence of streamers (narrow jets remaining after the passage of CME) is evident when the shock front passes through them. However, it is impossible now to establish unequivocal dependence between the jets' parameters (with all their variety) and the parameters of the separate fibers (their duration and radiation bandwidth). It is clear only that a certain agent must exist which propagates with a speed greater or less than the speed of the shock front in order that the drift speed of the fibers would also be more or less than the drift speed of the type II burst. To answer the question of the origin of fibers in the IP bursts, we will briefly summarize the known models and generation mechanisms of fiber bursts and the zebra pattern.

3.1. Generation Mechanisms

The interpretation of the complex fine structure of fibers and ZS has always lagged somewhat behind the detection of new, even more varied, observational phenomena. However, the most widespread model for fiber bursts is radio emission due to interactions between electrostatic plasma waves (l) and whistlers (w), both excited by the same population of fast electrons which has a loss-cone velocity distribution with the ordinary waves (t) freely escaping: $l + w \rightarrow t$ (Kuijpers, 1975a, 1975b). The version of the model in the framework of strong whistler turbulence was also developed by Bernold and Treumann (1983). Alfvénic solitons were also used for intermediate drift bursts (Treumann, Güdel, and Benz, 1990), as well as sausage modes (Kuznetsov, 2006).

The development of the theory of zebra pattern structures has been much more complicated. More than ten different models have been proposed, most of them including the emission of electrostatic plasma waves at the double plasma resonance (DPR) frequency (Kuijpers, 1975a; Zheleznykov and Zlotnik, 1975; Mollwo, 1983, 1988; Winglee and Dulk, 1986):

$$\omega_{\mathrm{UH}} = \left(\omega_{Pe}^2 + \omega_{Be}^2\right)^{1/2} = s\omega_{Be}, \tag{2}$$

where ω_{UH} is the upper-hybrid frequency, ω_{Pe} is the electron plasma frequency, ω_{Be} is the electron cyclotron frequency, and s is the harmonic number. The model that best describes the observations and the conditions in the corona is the model of Winglee and Dulk (1986),

which is based on nonsaturated electron-cyclotron maser emission by electrons with a loss-cone distribution. However, some difficulties remain with all of these versions, mainly the magnetic field deduced from Δf_s seems too low to have plasma $\beta \leq 1$ and occurrence of DPR in narrow flare loops causes doubt. LaBelle et al. (2003) proposed a mechanism of the leakage of the Z-mode from density enhancements at one DPR level in the form of eigenmodes similar to the auroral roar emissions in the terrestrial ionosphere. Although zebra pattern emission from a compact source was developed (by many authors) simultaneously with the DPR model: the process of nonlinear coupling of Bernstein cyclotron harmonics (Zheleznykov and Zlotnik, 1975). This mechanism is less effective and gives the extraordinary wave mode. In a number of recent papers, the DPR mechanism continues to be improved (Zlotnik et al., 2003).

The difficulties noted stimulated the search for other mechanisms. For example, Fomichev and Fainstein (1981) proposed the generation of the zebra pattern by the excitation of nonlinear ion-sound waves and their scattering on fast particles.

Long-term spectral fine structure observations reveal a number of features that cannot be easily described in the framework of existing mechanisms for the zebra structure. For instance, in a number of events, we observed quasi-parallel bands with a wave-like frequency drift; a continuous transition of zebra-structure stripes with wave-like drifts to typical IDB fibers with constant negative drift. The collected observational data suggest that the zebra structure bands and IDB fibers are related, and that their origin can be explained by a common mechanism, the interaction of plasma waves with whistlers: $l + w \rightarrow t$ (Chernov, 1976, 1996). The fibers are likely associated with ducted propagation of whistlers from the depths of the corona along a trap, while the zebra structure is associated with nonducted propagation oblique to the magnetic field, mainly at the top of the trap (Chernov, 1990, 2005).

3.2. Interpretation of the Fine Structure in IP Bursts

Let us note, that in almost all of the enumerated mechanisms, the electron cyclotron frequency (or its portion) is used as the harmonic frequency. Therefore it is possible to draw a conclusion that neither the frequency of whistler nor electronic cyclotron frequency determines the frequency bandwidth of the fibers or the frequency separation between them, since in the events discussed the observed values are greater by an order of magnitude. It is known that in the fronts of IP shocks whistlers are observed, and the CMEs represent magnetic clouds with the braided magnetic loops (flux-rope). Besides, it is possible to consider the presence of fast particles in front of the front as the obvious fact shown to be true by the occurrence of the SA bursts. The propagation of fronts through the elongated density heterogeneities (in the wake behind the CME) allows us to assume about an opportunity of generation of transition radiation which was already suggested as sources of the zebra patterns by LaBelle et al. (2003). In interplanetary space it should radiate much more effectively. The estimates of radio flux given in LaBelle et al. (2003) (their expression (15) on the basis of the formulas from Fleishman (2001)) show that the radio flux is proportional to the density contrast squared, $(\rho\%)^2$. If in the metric range, ρ can be only a few percent, in IP space the density contrast of jets may be more than twice the background density ($>100\%$). By varying other parameters the radio flux cannot be lower, (*e.g.*, in dependence on temperature and energy of electrons). The intensity of the transition radiation can be greatly enhanced by plasma resonance at frequencies just above the local plasma frequency (the resonance transition radiation (RTR)). RTR arises as fast particles move through a plasma with small scale variations (as short as the wavelength of the emitted wave) of the refractive index. Such variations may be provided by microturbulence-induced inhomogeneities

of the plasma density or magnetic field (Nita, Gary, and Fleishman, 2005). The RTR component is associated with a region of high density, and the RTR emission is *o*-mode polarized. Such conditions are indeed present in IP shock fronts propagating through the wake of a CME, especially regarding the occurrence of a resonance between the emitted wavelength and density irregularities.

A different frequency drift of fibers can arise from a different propagation angle of the shock front relative to jets with a high density gradient. But the main parameter, the total duration of each fiber, is determined by the time of the presence of fast particles on the boundary of two media with different density gradients. In the case of the shock front, this will be the transit time of the front through the heterogeneity, since the fast particles are present only directly in the front. This time depends on the difference between the speeds of the heterogeneity and the front. The shock front is absent in type III bursts, and the duration of striae is determined also by the time of the intersection of fast particles with heterogeneity. Fast particles of a type III beam fly away providing the emission of type III mainly from its forward edge, but the transition emission is excited throughout the entire beam length of the boundary of heterogeneity. Therefore striae have a somewhat larger duration in the comparison with the basic type III burst that we see on Figure 13. Thus, the frequency drift of fibers and striae is defined by the speed of the heterogeneity, which can be somewhat more or less than the speed of the shock front.

The transition of the herringbone structure for meter waves (to 25 MHz) into the large-scale and rather slowly drifting fibers becomes clear (17 September 2001, Figure 4). Small-scale (fast) details are no longer visible in the WIND spectrum, but at the same time the shock front entered into the region of heterogeneities behind the forward edge of the CME, the transition radiation from the heterogeneities becomes more intense. The drift velocity of the fibers between 12 and 5 MHz in Figure 4 corresponds to the velocity of heterogeneities $\sim$1400 km s^{-1} in the model of Leblanc, Dulk, and Bougeret (1998), close to speed of CME, which argues in favor of this model. The U bursts in Figure 4c have probably the same nature as in the 3 November 2003 event. The beginning of the ascending branch at 08.6 UT is joined with the type III burst. Therefore it is obvious that the type III beam was trapped in the magnetic cloud of the CME, and a portion of the fast particles was reflected back into the corona. According to the height-time diagram of the CME, it was located at the distance about 5 $R_{\odot}$ corresponding to the reflection frequency of 1.5 MHz.

On 13 November 2003 (Figure 8) we see another scenario of the fine structure. The fibers between 14 – 5 MHz are the continuation of metric fiber structure against the continuum emission, resulting in the propagating whistler wave packets. Only in IP space do we see some fibers (with harmonics) due to the transition radiation during the shock propagation through the CME wake (after CME overtook the shock front).

The fiber structure of the 2 May 1998 IP burst is not the direct continuation of fine structure from the meter range. The general view of the spectrum differs considerably; therefore the mechanism of their formation is different also, apparently. In that case, the fibers are the result of the propagation of the fronts along narrow density heterogeneities (seen in Figure 11), and we observe the maximum emission only from these structures (streamers after the passage of the CME). In such a case, the main contribution could give the transition radiation.

The discussed fibers are observed only at the selected frequency range 14 – 1 MHz. The absence of these fine structures in RAD1 and TNR spectra can be naturally explained by the considerable expansion of the CME in space and by the vanishing of the wakes, when heterogeneities are no longer encountered along the path of the shock fronts.

4. Conclusion

We have analyzed *WIND/WAVES* RAD2 spectra with fine structure in the form of different fibers in 14 events covering 1997 – 2005. A splitting of broad bands of IP type II bursts into narrow band fibers of different duration is observed. The instant frequency bandwidth of fibers is stable enough, 200 – 300 kHz for slow-drifting fibers in the type II burst, and 700 – 1000 kHz for fast-drifting fibers in the type II + IV (continuum). In addition, we have found neither the IP bursts with periodic and parallel-drifting fibers typical of meter and decimeter wave ranges nor the classical zebra pattern with variable frequency drift of stripes. Only the 19 April 2000 fibers in the range 2 – 1 MHz are somewhat similar to metric IDB, and on 13 November 2003 a set of fibers is somewhat similar to a rope of fibers in the metric range, but in both cases the scales of fiber parameters, and consequently of the source sizes in the IP space, are much larger.

In some events an expansion of metric fiber structure or herringbone structure into *WAVES* RAD2 spectra (14 – 5 MHz) was observed. In such cases the radio emission mechanism can be the same as in the metric range, mainly the modulation of radio continuum emission by whistler wave packets before the shock front (or between two shock fronts).

But in most of the events, with the splitting of the usual patch structure in IP type II (or II + IV) bursts into the narrow band fibers, the comparison of spectra with LASCO C2 images testifies to the passage of shock fronts at these moments through narrow jets in the wake of the CME. The propagation of fronts through the elongated density inhomogeneities (in the wake behind a CME), allows one to assume an opportunity of generation of transition radiation (actually resonance transition radiation), when the scales of the density variations in the jets are as short as the wavelength of the emitted wave. 300 m scales of inhomogeneities are very realistic over the distance $2-4\ R_{\odot}$.

More precise estimations for checking the proposed scheme of fiber formation in IP type II bursts could be made if we could obtain more reliable values of density and magnetic field inside a CME and the positions and sizes of the radio sources, which can be obtained by STEREO.

Acknowledgements We are grateful to Meudon, Nançay, and Culgoora (spectral data), SOHO (LASCO/EIT), and *WAVES* teams for operating the instruments and performing the basic data reduction, and especially, for the open data policy. The CME catalog is generated and maintained at the CDAW Data Center by NASA and the Catholic University of America in cooperation with the Naval Research Laboratory. SOHO is a project of international cooperation between ESA and NASA. The spectral data of the Nançay DCM spectrometer-polarimeter were kindly made available by A. Lecacheux. This study was supported in part by the Russian Foundation of Basic Research, grant No. 05-02-16271.

References

Bernold, T.E.X., Treumann, R.A.: 1983, *Astrophys. J.* **264**, 677.
Bougeret, J.-L., Kaiser, M.L. , Kellogg, P.J., *et al.: 1995, Space Sci. Rev.* ***71****, 5.*
Bougeret, J.-L., Zarka, P., Caroubalos, C., *et al.: 1998, Geophys. Res. Lett.* ***25****, 2513.*
Cane, H.V., Erickson, W.C.: 2005, *Astrophys. J.* **623**, 1180.
Chernov, G.P.: 1976, *Sov. Astron.* **20**, 582.
Chernov, G.P.: 1989, *Sov. Astron.* **33**, 649.
Chernov, G.P.: 1990, *Solar Phys.* **130**, 75.
Chernov, G.P.: 1996, *Astron. Rep.* **40**, 561.
Chernov, G.P.: 1997, *Astron. Lett.* **23**, 827.
Chernov, G.P.: 2005, *Plasma Phys. Rep.* **31**, 314.
Elgaroy, Ø.: 1959, *Nature* **184**, 887.
Fleishman, G.D.: 2001, *Astron. Lett.* **26**, 254.

Fomichev, V.V., Fainstein, S.M.: 1981, *Solar Phys.* **71**, 385.
Jiřička, K., Karlicky, M., Meszarosova, H., Snižek, V.: 2001, *Astron. Astrophys.* **375**, 243.
Kruger, A.: 1979, *Introduction to Solar Radio Astronomy and Radio Physics*, Reidel, Dordrecht.
Kuijpers, J.: 1975a, *Ph.D. Thesis*, Utrecht Univ.
Kuijpers, J.: 1975b, *Solar Phys.* **44**, 173.
Kuznetsov, A.A.: 2006, *Solar Phys.* **237**, 153.
LaBelle, J., Treumann, R.A., Yoon, P.H., Karlicky, M.: 2003, *Astrophys. J.* **593**, 1195.
Leblanc, Y., Dulk, G.A., Bougeret, J.-L.: 1998, *Solar Phys.* **183**, 165.
Leblanc, Y., Dulk, G.A., Cairns, I.H., Bougeret, J.-L.: 2000, *J. Geophys. Res.* **105**, 18215.
Mann, G., Baumgaertel, K., Chernov, G.P., Karlicky, M.: 1989, *Solar Phys.* **120**, 383.
Mollwo, L.: 1983, *Solar Phys.* **83**, 305.
Mollwo, L.: 1988, *Solar Phys.* **116**, 323.
Nita, G.M., Gary, D.E., Fleishman, G.D.: 2005, *Astrophys. J.* **629**, L65.
Reiner, M.J., Kaiser, M.L., Fainberg, J., Bougeret, J.-L.: 2006, *Solar Phys.* **234**, 301.
Slottje, C.: 1981, *Atlas of Fine Structures of Dynamic Spectra of Solar Type IV-dm and Some Type II Radio Bursts*, Utrecht Observatory.
Treumann, R.A., Güdel, M., Benz, A.O.: 1990, *Astron. Astrophys.* **236**, 242.
Winglee, R.M., Dulk, G.A.: 1986, *Astrophys. J.* **307**, 808.
Vrsnak, B., Warmuth, A., Temmer, M., Veronig, A., Magdalenich, J., Hillaris, A., Karlicky, M.: 2006, *Astron. Astrophys.* **448**, 739.
Zheleznykov, V.V., Zlotnik, E.Ya.: 1975, *Solar Phys.* **44**, 461.
Zlotnik, E.Ya., Zaitsev, V.V., Aurass, H., Mann, G., Hofmann, A.: 2003, *Astron. Astrophys.* **410**, 1011.